

Simulating triangle Hofstadter-Hubbard model with fermionic projected entangled simplex states

Sen Niu,^{1,*} D. N. Sheng,^{1,†} and Yang Peng^{1,2,‡}

¹*Department of Physics and Astronomy, California State University Northridge, California 91330, USA*

²*Institute of Quantum Information and Matter and Department of Physics,
California Institute of Technology, Pasadena, CA 91125, USA*

(Dated: December 29, 2025)

The triangular Hofstadter-Hubbard model, realizable in moiré bilayers, provides a fertile ground for discovering correlated topological states. We investigate this model in the grand canonical ensemble by introducing a fermionic infinite projected entangled simplex state (iPESS) approach, which offers direct access to the stability of the emergent correlated states at the thermodynamic limit. Through numerically optimizing fermionic iPESS, we accurately capture the chiral spin liquid (CSL) phase in the Mott insulating regime, characterized by a uniform chiral order, entanglement spectrum and the appearance of gossamer correlation tails in spin channel. The intermediate- U CSL is separated from the weak- U Chern insulator by a Mott transition at $U_{c_1} \approx 11.5$, signaled by changes in the charge fluctuation and compressibility. Finite-correlation-length scaling of the magnetization reveals a transition into a large- U 120° Néel phase at $U_{c_2} \approx 22.5$. Remarkably, with finite hole doping δ , we identify a uniform superconducting state with a finite pairing amplitude, whose order parameter displays a nearly universal phase winding across the U - δ phase diagram. Our work demonstrates robust chiral superconductivity in the thermodynamic limit through doping Chern insulator and CSL.

Introduction. A chiral spin liquid (CSL) is a topological quantum phase formed by highly entangled spins that breaks time-reversal symmetry and supports anyonic excitations [1–3]. As the bosonic analogue of the fractional quantum Hall state [1], the CSL has long been a central target in the search for strongly correlated topological matter [4–9]. Recently, a triangular Hofstadter-Hubbard model proposed in moiré bilayer structures [10] with finite magnetic flux, emerges as a promising platform to realize a CSL by driving a spinful Chern insulator (CI) into the Mott regime [11, 12]. Even more intriguingly, theoretical and numerical studies indicate that doping near the Mott transition yields chiral superconductivity (SC), as evidenced by the calculated pairing binding energies [13] and dominant power-law pairing correlations [14, 15]. To date, however, these key signatures of the Mott transition and the associated SC have been observed primarily in density matrix renormalization group (DMRG) [16] and Monte-Carlo simulations on finite-width cylinders [10–15]. The stability of chiral SC and the competing charge density wave order in the thermodynamic limit remain crucial open questions.

Infinite projected entangled pair state [17] (iPEPS) is an entanglement-based tensor network ansatz for simulating two-dimensional strongly correlated systems on an *infinite* lattice. Its fermionic generalization [18–24] has demonstrated to be a powerful tool for studying SC and other competing symmetry breaking orders in standard $t - J$ and Hubbard models with time-reversal symmetry [25–37], allowing thermodynamic detection of pairing order parameters in the grand canonical ensemble. However, whether iPEPS can simulate the chiral SC and even its parent CSL state in the Mott regime of fermionic Hubbard models remains an open question. The challenge originates from the topological obstruction inherent to chiral topological states [38], which carry nonzero (many-body) Chern numbers and cannot be Wannierized [39]. This appears to contradict the local tensor structure of PEPS. A no-

go theorem for free-fermion Chern insulators [38, 40] establishes that Gaussian fermionic PEPS can indeed carry non-zero Chern numbers, but their correlation functions necessarily exhibit power-law decay, mimicking gapless behavior. Subsequent iPEPS wavefunction studies found similar artifact in CSL correlation functions [41, 42]. Despite this conceptual obstruction, variational optimization studies demonstrated that, upon increasing the bond dimension, these unphysical correlations become confined to longer length scales and gradually weaken with increasing bond dimension, forming a so-called “gossamer tail” [43, 44]. Further wavefunction overlap calculations reveal that the presence of such gossamer tails does not obstruct PEPS from correctly capturing chiral topological degeneracy [45]. Beyond these conceptual benchmarks, the practical power of iPEPS is further demonstrated by its successful application to CSLs in a broad class of spin [46–54] and bosonic [55, 56] correlated lattice Hamiltonians.

Along this direction, the understanding of the iPEPS representation for chiral topological states in fermionic systems remains primitive, as numerical studies so far have been limited to spinless Chern insulators [38, 44, 57, 58]. A critical open question is whether iPEPS can accurately describe the elusive CSL phase in strongly correlated Mott insulators in the presence of charge fluctuations, strong interplay between the charge and spin degrees of freedom, and larger local Hilbert space [13, 59, 60]. Furthermore, another challenge is to simulate doped topological phases and directly probe the emergence of SC via order parameters in the grand canonical ensemble for infinite systems, which remains unexplored so far [10–15].

In this Letter, we introduce a fermionic infinite projected entangled simplex state (iPESS) method [61, 62] as a generalized fermionic iPEPS to simulate the triangular Hofstadter-Hubbard model [Fig. 1(a-c)]. The key ingredients of our approach are: (i) a fermionic simplex ansatz that treats all tri-

angle edges on equal footing, and (ii) the variational optimization or full-update of tensors that incorporates long-range correlation effects, which is crucial for accurate simulations. Using large-scale simulations, we study the $\pi/2$ -flux model in the grand canonical ensemble for infinite system. From the convergence of variational energy, the fingerprint entanglement spectrum, and the characteristic ‘‘gossamer tails’’ in correlation functions, we find that the fermionic iPESS ansatz faithfully represents the intermediate- U CSL at finite bond dimensions we can access. The Mott transition between the incompressible CI and the CSL is identified from the evolution of the charge susceptibility and double occupancy, while the magnetic transition from the CSL to the 120° Néel phase is located via finite-correlation-length scaling of the magnetization on infinite lattice. Crucially, upon doping the half-filled insulating states, we uncover uniform SC phases with complex pairing order parameters, where the pairing field exhibits a anti-clockwise phase winding in a broad regime in the δ - U plane except near the Mott criticality [Fig. 1 (d)]. Our work unravels chiral SC and establishes fermionic iPESS as an effective tool for studying such states in thermodynamic limit.

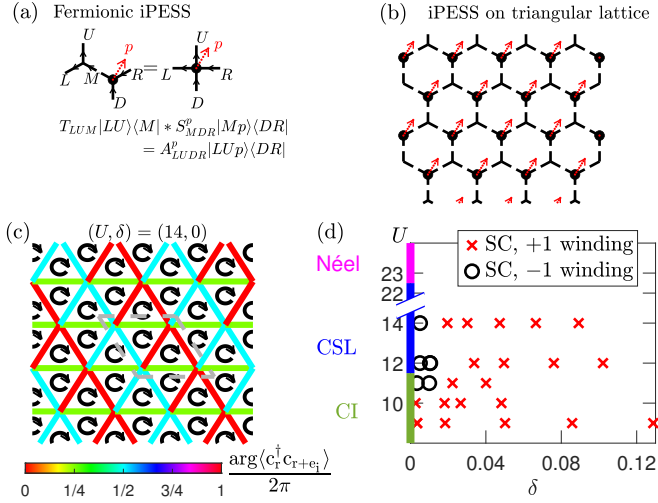


FIG. 1. **Fermionic iPESS ansatz and phase diagram.** (a) Fermionic simplex tensors for a single site. (b) Fermionic iPESS on the infinite lattice. (c) Symmetry quality of optimized fermionic iPESS for $D = 8$: bond thickness and color indicate hopping amplitudes and phases; black circle arrows indicate scalar chirality magnitudes; dashed lines mark the 2×2 cell of iPESS. (d) Phase diagrams for the insulating $\delta = 0$ and hole-doped $\delta > 0$ regimes.

Model and fermionic iPESS Method. The spin-1/2 grand canonical Hofstadter-Hubbard Hamiltonian is defined as

$$H = \sum_{\langle i,j \rangle, \sigma} (t_{ij} c_{i\sigma}^\dagger c_{j\sigma} + \text{h.c.}) + U \sum_i (n_{i\uparrow} - \frac{1}{2})(n_{i\downarrow} - \frac{1}{2}) - \mu \sum_{i,\sigma} n_{i\sigma} \quad (1)$$

on the triangular lattice with primitive translation vectors $e_1 = (1, 0)$, $e_2 = (-1/2, \sqrt{3}/2)$, $e_3 = e_1 + e_2$. Each triangle is pierced by $\pi/2$ magnetic flux, and we adopt the gauge

$t_{r,r+e_1} = it$, $t_{r,r+e_2} = (-1)^x t$, $t_{r,r+e_3} = (-1)^{x-1} t$ from Ref. [10], where $r = (x, y)$ and $t = 1$. In the non-interacting limit, the model has a 2×1 unit-cell and exhibits a pair of particle-hole symmetric $C = \pm 1$ Chern bands. The average filling fraction $\nu = 1 - \delta$ is tuned by chemical potential μ , with $\mu = 0$ giving half-filling $\nu = 1$ due to particle-hole symmetry.

To tackle the fermionic model on the infinite triangular lattice, we introduce the fermionic iPESS ansatz, which combines the simplex structure [61–63] with fermionic tensor techniques [18–23]. We define a rank-3 virtual simplex $\hat{T} = T_{LUM}|LU\rangle\langle M|$ tensor at the center of each up-triangle and a rank-4 physical $\hat{S} = S_{MDR}^p|Mp\rangle\langle DR|$ tensor on each lattice site, as shown in Fig. 1 (a)-(b). Here L, D, R, U, M denote virtual fermionic modes with bonds dimension D , and p indexes the four-dimensional local Hubbard Hilbert space. Imposing Z_2 fermion parity symmetry in both tensors and Hamiltonian operators avoids non-local Jordan-Wigner strings on the infinite 2D lattice. Contracting the M index between neighboring \hat{T} and \hat{S} tensors shows that iPESS is a subclass of standard iPEPS, with the simplex structure treating entanglement among three sites within a triangle equally and better preserving point group symmetries.

Due to the high computational cost of the Hubbard model, we adopt spin-SU(2) symmetric tensors without fixing particle numbers in the grand canonical ensemble. Translation-invariant $m \times n$ unit-cells (with even m) are imposed on the infinite lattice. We optimize SU(2)-invariant tensors using gradient descent variational optimization for moderate $D \leq 8$, with the gradients given by automatic differentiation [64]. To further increase the SU(2) virtual bonds and improve energies, we perform full-update [65] via imaginary-time evolution. In both variational and full-update methods, the environments of bulk tensors are obtained by the corner-transfer-matrix renormalization group (CTMRG) method [26, 66], which approximately contracts iPESS from an effectively infinite boundary to the bulk. In Supplemental Materials (SM) [67], we show that the CTMRG environment that incorporates long-range correlations from gossamer tails is essential for accurate simulation, as the computationally cheaper simple-update method [68] retains only local environments and fails to reach lower energy regime.

Weak- U Chern insulator and intermediate- U Chiral spin liquid. At half filling, two chiral topological states are expected based on DMRG simulations[10]. The weak- U CI phase persists due to finite band gap, while in the Mott insulating regime with moderate U , electron hopping is suppressed and spin interactions dominant the physics via higher-order virtual processes. We first check the convergence of our 2×2 iPESS ansatz for such strongly correlated systems. The finite- D energies per site for $U = 8, 14$ are shown in Fig. 2 (a)-(b), where the χ_{iPESS} denotes the CTMRG environment dimension controlling the contraction accuracy. iPESS energy converges with increasing bond dimension while infinite DMRG energy converges from below with increasing cylinder width L_y , both towards close values demonstrating good convergence for both methods. The phases of nearest-

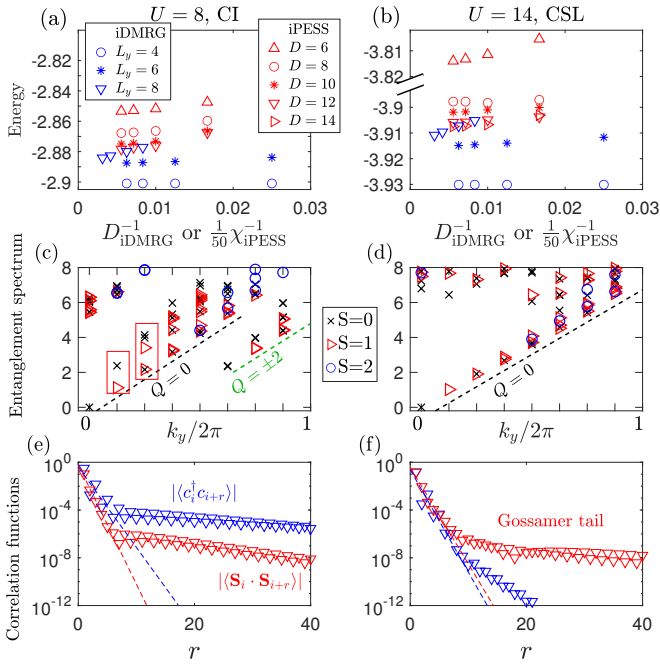


FIG. 2. **Weak- U CI and intermediate- U CSL phases.** (a)-(b) Energy convergence for finite- D iPESS and iDMRG on cylinders of width L_y . (c)-(d) iPESS entanglement spectrum for $(D, \chi_{\text{iPESS}}) = (12, 60)$. (e)-(f) iPESS correlation functions for $(D, \chi_{\text{iPESS}}) = (12, 160)$.

neighbor (NN) hopping $\arg\langle c_r^\dagger c_{r+e_i} \rangle$ indicated by bond color in Fig. 1(c) match with the complex hopping terms in Eq. (1). The nearly uniform NN hopping amplitudes $|\langle c_r^\dagger c_{r+e_i} \rangle|$ (indicated by bond thickness) and scalar chirality $\langle \chi_{ijk} \rangle = \langle \mathbf{S}_i \cdot (\mathbf{S}_j \times \mathbf{S}_k) \rangle$ (indicated by size of black circular arrows) in Fig. 1(c) shows that the triangular lattice symmetry is well preserved by iPESS.

Topological properties of chiral states are reflected in the entanglement spectrum (ES) via the Li-Haldane conjecture [69]. We compute ES by placing our system with 2×2 cells on finite-width cylinders [70–72] after optimizing iPESS. The algorithm for calculating ES with fermionic iPESS using CTMRG environments is presented in SM [67]. ES on a width-8 cylinder are shown in Fig. 2(c)-(d). For $U = 8$, charge fluctuations are not strongly suppressed, as seen by the dominant $Q = 0$ branch and the degenerate $Q = \pm 2$ branches marked by charge Q . Low-lying levels of a single branch match the spinful CI pattern $0, 0 \oplus 1, 3(0) \oplus 2(1), \dots$ in $SU(2)$ representation. For $U = 14$ and large enough bond dimensions $D \geq 8$, a single low-lying branch identifies the Kalmeyer-Laughlin CSL, with reduced level counting $0, 1, 0 \oplus 1, 0 \oplus 2(1), \dots$ agreeing with $SU(2)_1$ conformal field theory [73]. The topological obstruction for fermionic iPESS appears in correlations [Fig. 2(e)-(f)]: for CI, all channels show exponential-decay at short distances followed by slower-decay gossamer tails at long distances. For CSL, only spin-spin correlations exhibit clear gossamer tails, consistent with topological spin degrees of freedom in a Mott insulator.

These signatures confirm that fermionic iPESS faithfully represents both topological CI and CSL.

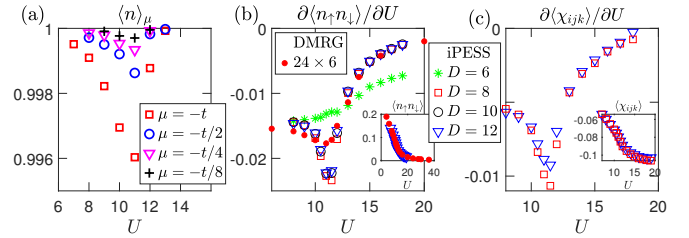


FIG. 3. **Signatures of Mott transition between CI and CSL.** (a) Deviation from half-filling $n = 1$ for negative chemical potential μ . (b)-(c) Double occupancy $\langle n_{i\uparrow} n_{i\downarrow} \rangle$ and scalar chirality $\langle \chi_{ijk} \rangle$ and their derivatives versus U at half filling.

Mott transition between weak and intermediate U . We further determine the critical U_{c1} between CI and CSL. We first examine the sensitivity of the average particle number $\bar{n} = \langle n \rangle_\mu$ to chemical potential μ [Fig. 3(a)]. Ref. [13] proposes a transition between band and Mott insulators at U_{c1} , where the charge- $2e$ gap closes while the spin gap remains open. The occupation \bar{n} exhibits a minimum near $U_{c1} \sim 11.5$, rapidly approaching 1 as $\mu \rightarrow 0$ on both sides. We identify U_{c1} as the critical point since CI and Mott insulators are incompressible ($\chi_e = \partial \bar{n} / \partial \mu = 0$) except at gap closure. Double occupancy, reflecting charge fluctuations via $\langle n_{i\uparrow} n_{i\downarrow} \rangle = \langle (n - \bar{n})^2 \rangle / 2$ for $\bar{n} = 1$, shows a sudden suppression at U_{c1} , with a singularity in its derivative for iPESS $D \geq 8$ and DMRG results [Fig. 3(b)]. The scalar chirality χ_{ijk} , nonzero due to time-reversal symmetry breaking, also exhibits a derivative singularity at U_{c1} [Fig. 3(c)].

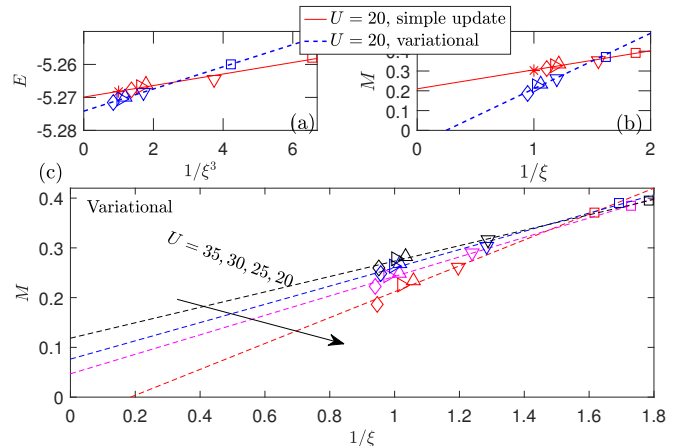


FIG. 4. **Magnetic transition at half-filling via finite-correlation-length scaling.** Z_2 symmetric 6×6 iPESS ansatz is used. The square, down-triangle, up-triangle, right-triangle, diamond, star symbols correspond to bond dimensions $D = 6, 7, 8, 9, 10, 12$. (a)-(b) Energy and magnetization comparison between simple-update and variational optimization. (c) Extrapolated magnetization vs. U from variational optimization.

Magnetic transition between intermediate and large U . In

the large- U limit, the Hofstadter-Hubbard model reduces to an effective NN Heisenberg model, favoring 120° Néel order [74, 75]. We determine the critical point between the intermediate- U CSL and large- U magnetic phase. As Néel order spontaneously breaks spin-rotation symmetry in 2D infinite system, the correlation length of spin-spin correlations in the Néel phase diverge. In infinite tensor network simulations, finite bond dimensions limits the correlation length, making finite-correlation-length scaling of magnetization important [76–80]. We perform Z_2 symmetric iPESS simulations with a unit cell 6×6 which accommodates 120° Néel order. Although such large cell is typically challenging for variational optimization due to memory demands, the rank-3 structure of iPESS tensors costs much less memory than rank-4 iPEPS and thus enables simulation up to $D = 10$.

Energy and magnetization versus correlation length ξ at $U = 20$ are shown in Fig. 4(a)-(b). We analyze the data based on the empirical scaling hypothesis [80] for 120° Néel order

$$E(\xi) = E(\infty) + a/\xi^3, \\ M(\xi) = M(\infty) + b/\xi, \quad (2)$$

where E scales linearly with $1/\xi^3$ and M with $1/\xi$, respectively. The accurate variational data extrapolates to negative M at $U = 20$, indicating a non-magnetic CSL phase. The finite- D magnetization suggests proximity to a gapless critical point, similar to gapless spin liquids [81] where symmetry breaking can lower energy in restricted variational spaces. This highlights the importance of full variational optimization: a simple-update incorrectly yields a magnetic order and overestimated M [Fig. 4(a)-(b)].

Magnetization for different U values appears in Fig. 4(c). At $U = 20$, magnetization scales negatively, while at $U = 25, 30, 35$, it scales to a positive value at $1/\xi \rightarrow 0$ limit, which increases with U . The magnetic critical point is identified as $U_{c_2} \approx 22.5$ roughly consistent with estimates from the effective $J - J_\chi$ spin model [10, 13, 74, 75]. These results confirm the CSL as a robust phase for a wide parameter regime in thermodynamic limit in the Hofstadter-Hubbard model, contrasting with the narrow CSL regime in the standard triangular Hubbard model [82–84].

Chiral superconductivity at finite hole doping. We now investigate possible SC in the lightly hole-doped regime near the Mott transition U_{c_1} . To efficiently simulate finite- δ states, we adopt $SU(2)$ symmetric 2×2 iPESS ansatz, and take optimized solutions at half-filling as initial states for gradient optimization. Under the original gauge of Ref. [10] with a 2×1 unit cell, iPESS solutions exhibit staggered NN pairing along y , yielding 2×2 periodicity. For comparison with previous DMRG studies [10–15], we perform a gauge transformation to a C_6 symmetric imaginary gauge with a 2×2 unit cell [67].

The typical NN pairing pattern $\Delta_i(\mathbf{r}) = \langle c_{\mathbf{r},\uparrow}^\dagger c_{\mathbf{r}+\mathbf{e}_i,\downarrow}^\dagger - c_{\mathbf{r},\downarrow}^\dagger c_{\mathbf{r}+\mathbf{e}_i,\uparrow}^\dagger \rangle / \sqrt{2}$ is shown in Fig. 5(a), where the bond thickness is proportional to square root of pairing amplitude $\sqrt{|\Delta|}$. Phases on NN bonds exhibit uniform anticlockwise +1 wind-

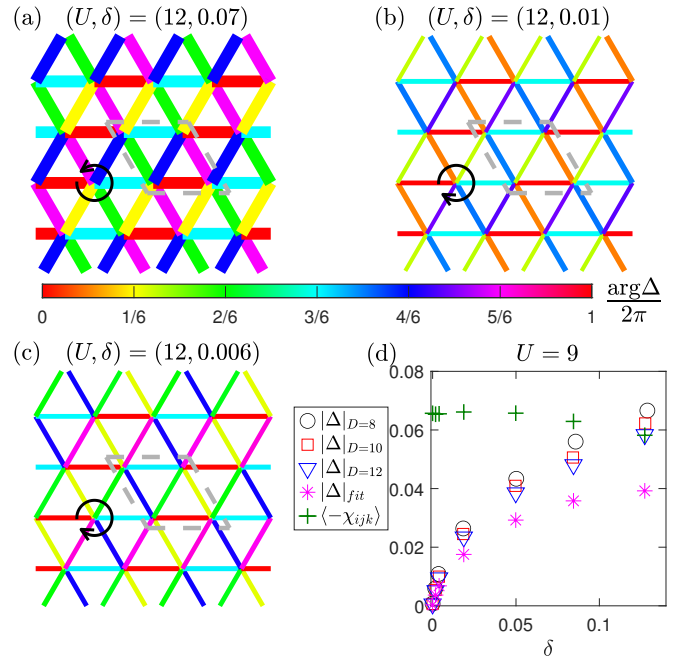


FIG. 5. SC pairing symmetry and strength versus hole doping δ . (a)-(c) Phases (color) and magnitudes (bond thickness) of pairing Δ under C_6 imaginary gauge with $U = 12, D = 12$. The bond thickness is proportional to square root of pairing amplitude $\sqrt{|\Delta|}$. Black circular arrows indicate the phase winding. (d) Spin chirality and Δ strength vs. δ , with $1/D$ extrapolation for $U = 9$.

ing. As indicated in the phase diagram [Fig. 1(d)], this pattern is universal across a broad U - δ range, consistent with pair-pair correlations of numerical simulations in the canonical ensemble [13–15]. Upon reducing doping and approaching $U = U_{c_1}$, the NN pairing undergoes a crossover [Fig. 5(b)] with a non- C_6 -symmetric distribution of pairing phases, eventually developing uniform SC with clockwise -1 winding at very low doping $\delta < 0.01$ [Fig. 5(c)]. The clockwise -1 winding SC phase shares similar scalar spin chirality and entanglement spectrum with both the CSL phase and the anti-clockwise $+1$ winding SC phase. The microscopic origin and physical implications of this winding-number reversal remain open questions and warrant further investigation.

We further show finite- D and $1/D$ linearly extrapolated NN pairing amplitude $|\Delta|$ at $U = 9$ in Fig. 5(d), where we find $|\Delta|$ remains finite over a wide doping range and increases with doping in the range of $0 < \delta \leq 0.15$. We also confirm that the SC phase is a robust ground state in Z_2 symmetric 4×4 iPESS simulations, with no charge density wave or magnetic order for this doping range [67]. The lightly doped regime also shows universal gossamer tails in correlations and finite spin chiralities $\langle \chi_{ijk} \rangle$, consistent with chiral topological SC [14, 15]. Our iPESS simulations confirm chiral SC as a robust ground state in the thermodynamic limit.

Conclusion. In summary, we have introduced a fermionic iPESS approach that enables accurate simulation of the triangular Hofstadter-Hubbard model and a quantitative identi-

fication of chiral SC upon doping. Our method successfully captures the elusive CSL in the presence of charge fluctuations, as rigorously validated by its variational energy, entanglement spectrum, and gossamer tails. By locating both the Mott transition separating the CSL from the CI and the magnetic transition between the CSL and Néel order, we establish the stability of the CSL phase across a broad parameter range. Crucially, we demonstrate finite SC pairing orders over a wide U - δ region, with a pairing symmetry consistent with prior studies, and predict a small pocket with opposite phase winding near the Mott criticality. This work provides compelling evidence for robust chiral SC emerging in the thermodynamic limit from doping both Chern insulator and CSL.

Acknowledgment. Sen Niu is thankful for insightful discussion with Didier Poilblanc, Leon Balents, Rong-Yang Sun, Jheng-Wei Li, Wen-Yuan Liu, Rui-Zhen Huang and Juraj Hasik. The research was supported by the U.S. Department of Energy, Office of Basic Energy Sciences under Grant No. DE-FG02-06ER46305 (SN, DNS) for numerical study of strongly correlated topological phases. This work is also supported by the US National Science Foundation (NSF) Grant No. PHY-2216774 (YP). The numerical simulation is partially supported by NSF instrument grant DMR-2406524, and TensorKit.jl [85] and YASTN [86] packages are used for automatic differentiation with $SU(2)$ and Z_2 symmetric tensors, respectively.

* sen.niu@csun.edu
 † donna.sheng@csun.edu
 ‡ yang.peng@csun.edu

[1] V. Kalmeyer and R. Laughlin, Equivalence of the resonating-valence-bond and fractional quantum hall states, *Physical review letters* **59**, 2095 (1987).
 [2] V. Kalmeyer and R. Laughlin, Theory of the spin liquid state of the heisenberg antiferromagnet, *Physical Review B* **39**, 11879 (1989).
 [3] X.-G. Wen, F. Wilczek, and A. Zee, Chiral spin states and superconductivity, *Physical Review B* **39**, 11413 (1989).
 [4] D. F. Schroeter, E. Kapit, R. Thomale, and M. Greiter, Spin hamiltonian for which the chiral spin liquid is the exact ground state, *Physical review letters* **99**, 097202 (2007).
 [5] A. E. Nielsen, J. I. Cirac, and G. Sierra, Laughlin spin-liquid states on lattices obtained from conformal field theory, *Physical review letters* **108**, 257206 (2012).
 [6] Y.-C. He, D. Sheng, and Y. Chen, Chiral spin liquid in a frustrated anisotropic kagome heisenberg model, *Physical review letters* **112**, 137202 (2014).
 [7] S.-S. Gong, W. Zhu, and D. Sheng, Emergent chiral spin liquid: Fractional quantum hall effect in a kagome heisenberg model, *Scientific reports* **4**, 6317 (2014).
 [8] B. Bauer, L. Cincio, B. P. Keller, M. Dolfi, G. Vidal, S. Trebst, and A. W. Ludwig, Chiral spin liquid and emergent anyons in a kagome lattice mott insulator, *Nature communications* **5**, 5137 (2014).
 [9] X.-J. Liu, Z.-X. Liu, K. Law, W. V. Liu, and T. Ng, Chiral topological orders in an optical raman lattice, *New Journal of Physics* **18**, 035004 (2016).
 [10] C. Kuhlenkamp, W. Kadow, A. Imamoğlu, and M. Knap, Chiral pseudospin liquids in moiré heterostructures, *Physical Review X* **14**, 021013 (2024).
 [11] S. Divic, T. Soejima, V. Crépel, M. P. Zaletel, and A. Millis, Chiral spin liquid and quantum phase transition in the triangular lattice hofstadter-hubbard model, *arXiv preprint arXiv:2406.15348* (2024).
 [12] C. A. Gallegos, R. M. Magaldi, A. Millis, and S. R. White, Quantum hall to chiral spin liquid transition in a triangular lattice hofstadter-hubbard model, *arXiv preprint arXiv:2510.19907* (2025).
 [13] S. Divic, V. Crépel, T. Soejima, X.-Y. Song, A. J. Millis, M. P. Zaletel, and A. Vishwanath, Anyon superconductivity from topological criticality in a hofstadter-hubbard model, *Proceedings of the National Academy of Sciences* **122**, e2426680122 (2025).
 [14] F. Chen, W. O. Wang, J.-X. Zhang, L. Balents, and D. Sheng, Topological chiral superconductivity in the triangular-lattice hofstadter-hubbard model, *arXiv preprint arXiv:2509.02757* (2025).
 [15] C. Kuhlenkamp, S. Divic, M. P. Zaletel, T. Soejima, and A. Vishwanath, Robust superconductivity upon doping chiral spin liquid and chern insulators in a hubbard-hofstadter model, *arXiv preprint arXiv:2509.02675* (2025).
 [16] S. R. White, Density matrix formulation for quantum renormalization groups, *Physical review letters* **69**, 2863 (1992).
 [17] F. Verstraete and J. I. Cirac, Renormalization algorithms for quantum-many body systems in two and higher dimensions, *arXiv preprint cond-mat/0407066* (2004).
 [18] T. Barthel, C. Pineda, and J. Eisert, Contraction of fermionic operator circuits and the simulation of strongly correlated fermions, *Physical Review A* **80**, 042333 (2009).
 [19] C. V. Kraus, N. Schuch, F. Verstraete, and J. I. Cirac, Fermionic projected entangled pair states, *Physical Review A—Atomic, Molecular, and Optical Physics* **81**, 052338 (2010).
 [20] Z.-C. Gu, F. Verstraete, and X.-G. Wen, Grassmann tensor network states and its renormalization for strongly correlated fermionic and bosonic states (2010), *arXiv preprint arXiv:1004.2563*.
 [21] I. Pižorn and F. Verstraete, Fermionic implementation of projected entangled pair states algorithm, *Physical Review B—Condensed Matter and Materials Physics* **81**, 245110 (2010).
 [22] P. Corboz, R. Orús, B. Bauer, and G. Vidal, Simulation of strongly correlated fermions in two spatial dimensions with fermionic projected entangled-pair states, *Physical Review B* **81**, 165104 (2010).
 [23] Z.-C. Gu, Efficient simulation of grassmann tensor product states, *Physical Review B—Condensed Matter and Materials Physics* **88**, 115139 (2013).
 [24] Y. Ma, S. Jiang, and C. Xu, Variational tensor wave functions for the interacting quantum spin hall phase, *Physical Review Letters* **132**, 126504 (2024).
 [25] P. Corboz, S. R. White, G. Vidal, and M. Troyer, Stripes in the two-dimensional t-j model with infinite projected entangled-pair states, *Physical Review B—Condensed Matter and Materials Physics* **84**, 041108 (2011).
 [26] P. Corboz, T. M. Rice, and M. Troyer, Competing states in the t-j model: Uniform d-wave state versus stripe state, *Phys. Rev. Lett.* **113**, 046402 (2014).
 [27] D. Poilblanc, P. Corboz, N. Schuch, and J. I. Cirac, Resonating-valence-bond superconductors with fermionic projected entangled pair states, *Physical Review B* **89**, 241106 (2014).
 [28] P. Corboz, Improved energy extrapolation with infinite pro-

jected entangled-pair states applied to the two-dimensional hubbard model, *Physical Review B* **93**, 045116 (2016).

[29] S.-J. Dong, C. Wang, Y.-J. Han, C. Yang, and L. He, Stable diagonal stripes in the t-j model at $n_h = 1/8$ doping from fpeps calculations, *npj Quantum Materials* **5**, 28 (2020).

[30] Z.-T. Xu, Z.-C. Gu, and S. Yang, Competing orders in the honeycomb lattice t-j model, *Physical Review B* **108**, 035144 (2023).

[31] Q. Yang, X.-Y. Zhang, H.-J. Liao, H.-H. Tu, and L. Wang, Projected d-wave superconducting state: A fermionic projected entangled pair state study, *Physical Review B* **107**, 125128 (2023).

[32] B. Ponsioen, S. S. Chung, and P. Corboz, Superconducting stripes in the hole-doped three-band hubbard model, *Physical Review B* **108**, 205154 (2023).

[33] W. Zheng, Z.-Y. Yue, J.-H. Zhang, and Z.-C. Gu, Competing pair density wave orders in the square lattice $t-j$ model, *arXiv preprint arXiv:2411.19218* (2024).

[34] W. Zheng, J.-X. Zhang, Z.-Y. Yue, Z.-C. Gu, and Z.-Y. Weng, Revealing quantum phase string effect in doped mott-insulator: a tensor network state approach, *arXiv preprint arXiv:2503.23851* (2025).

[35] W. Zheng, T. Cheng, Z.-Y. Yue, F.-C. Zhang, W.-Q. Chen, and Z.-C. Gu, Competing s -wave pairing in overdoped $t-j$ model, *arXiv preprint arXiv:2509.22473* (2025).

[36] C. Zhang, J.-W. Li, D. Nikolaïdou, and J. von Delft, Frustration-induced superconductivity in the $t-t'$ hubbard model, *Physical Review Letters* **134**, 116502 (2025).

[37] W.-Y. Liu, H. Zhai, R. Peng, Z.-C. Gu, and G. K.-L. Chan, Accurate simulation of the hubbard model with finite fermionic projected entangled pair states, *Physical Review Letters* **134**, 256502 (2025).

[38] T. B. Wahl, H.-H. Tu, N. Schuch, and J. I. Cirac, Projected entangled-pair states can describe chiral topological states, *Physical review letters* **111**, 236805 (2013).

[39] N. Marzari, A. A. Mostofi, J. R. Yates, I. Souza, and D. Vanderbilt, Maximally localized wannier functions: Theory and applications, *Reviews of Modern Physics* **84**, 1419 (2012).

[40] J. Dubail and N. Read, Tensor network trial states for chiral topological phases in two dimensions and a no-go theorem in any dimension, *Physical Review B* **92**, 205307 (2015).

[41] S. Yang, T. B. Wahl, H.-H. Tu, N. Schuch, and J. I. Cirac, Chiral projected entangled-pair state with topological order, *Physical review letters* **114**, 106803 (2015).

[42] D. Poilblanc, J. I. Cirac, and N. Schuch, Chiral topological spin liquids with projected entangled pair states, *Physical Review B* **91**, 224431 (2015).

[43] J. Hasik, M. Van Damme, D. Poilblanc, and L. Vanderstraeten, Simulating chiral spin liquids with projected entangled-pair states, *Physical Review Letters* **129**, 177201 (2022).

[44] S. Niu, J.-W. Li, J.-Y. Chen, and D. Poilblanc, Chiral spin liquids with projected gaussian fermionic entangled pair states, *Physical Review B* **109**, L081107 (2024).

[45] S. Budaraju, D. Poilblanc, and S. Niu, Simulating chiral spin liquids with fermionic projected entangled pair states, *Physical Review B* **110**, 064402 (2024).

[46] J.-Y. Chen, L. Vanderstraeten, S. Capponi, and D. Poilblanc, Non-abelian chiral spin liquid in a quantum antiferromagnet revealed by an ipeps study, *Physical Review B* **98**, 184409 (2018).

[47] J.-Y. Chen, S. Capponi, A. Wietek, M. Mambrini, N. Schuch, and D. Poilblanc, Su (3) 1 chiral spin liquid on the square lattice: A view from symmetric projected entangled pair states, *Physical review letters* **125**, 017201 (2020).

[48] J.-Y. Chen, J.-W. Li, P. Nataf, S. Capponi, M. Mambrini, K. Totsuka, H.-H. Tu, A. Weichselbaum, J. von Delft, and D. Poilblanc, Abelian su (n) 1 chiral spin liquids on the square lattice, *Physical Review B* **104**, 235104 (2021).

[49] R. Wang, Z. Xie, B. Wang, and T. Sedrakyan, Emergent topological orders and phase transitions in lattice chern-simons theory of quantum magnets, *Physical Review B* **106**, L121117 (2022).

[50] S. Niu, J. Hasik, J.-Y. Chen, and D. Poilblanc, Chiral spin liquids on the kagome lattice with projected entangled simplex states, *Physical Review B* **106**, 245119 (2022).

[51] Y. Xu, S. Capponi, J.-Y. Chen, L. Vanderstraeten, J. Hasik, A. H. Nevidomskyy, M. Mambrini, K. Penc, and D. Poilblanc, Phase diagram of the chiral su (3) antiferromagnet on the kagome lattice, *Physical Review B* **108**, 195153 (2023).

[52] Y. Tan, J.-Y. Chen, D. Poilblanc, F. Ye, and J.-W. Mei, 1-form symmetric projected entangled-pair states, *arXiv preprint arXiv:2407.16531* (2024).

[53] D. A. Puente, E. L. Weerda, K. Schröder, and M. Rizzi, Efficient optimization and conceptual barriers in variational finite projected entangled pair states, *Physical Review B* **111**, 195120 (2025).

[54] J.-Y. Chen, Y. Tan, S. Capponi, D. Poilblanc, F. Ye, and J.-W. Mei, Simulating bulk gap in chiral projected entangled-pair states, *arXiv preprint arXiv:2502.20142* (2025).

[55] E. L. Weerda and M. Rizzi, Fractional quantum hall states with variational projected entangled-pair states: A study of the bosonic harper-hofstadter model, *Physical Review B* **109**, L241117 (2024).

[56] S. Dong, C. Wang, H. Zhang, M. Zhang, and L. He, Efficient projected entangled pair states methods for periodic quantum systems, *Physical Review Letters* **135**, 026501 (2025).

[57] Z. Dai, Y. Wu, T. Wang, and M. P. Zaletel, Fermionic isometric tensor network states in two dimensions, *Physical Review Letters* **134**, 026502 (2025).

[58] Y. Wu, Z. Dai, S. Anand, S.-H. Lin, Q. Yang, L. Wang, F. Pollmann, and M. P. Zaletel, Alternating and gaussian fermionic isometric tensor network states, *arXiv preprint arXiv:2502.10695* (2025).

[59] P. A. Lee, N. Nagaosa, and X.-G. Wen, Doping a mott insulator: Physics of high-temperature superconductivity, *Reviews of modern physics* **78**, 17 (2006).

[60] J. Yang and X.-J. Liu, Chiral spin liquid phase in an optical lattice at mean-field level, *Physical Review B* **109**, 165108 (2024).

[61] Z.-Y. Xie, J. Chen, J. Yu, X. Kong, B. Normand, and T. Xiang, Tensor renormalization of quantum many-body systems using projected entangled simplex states, *Phys. Rev. X* **4**, 011025 (2014).

[62] Q. Li, H. Li, J. Zhao, H.-G. Luo, and Z. Xie, Magnetization of the spin-1/2 heisenberg antiferromagnet on the triangular lattice, *Physical Review B* **105**, 184418 (2022).

[63] N. Schuch, D. Poilblanc, J. I. Cirac, and D. Pérez-García, Resonating valence bond states in the peps formalism, *Physical Review B—Condensed Matter and Materials Physics* **86**, 115108 (2012).

[64] H.-J. Liao, J.-G. Liu, L. Wang, and T. Xiang, Differentiable programming tensor networks, *Phys. Rev. X* **9**, 031041 (2019).

[65] J. Jordan, R. Orús, G. Vidal, F. Verstraete, and J. I. Cirac, Classical simulation of infinite-size quantum lattice systems in two spatial dimensions, *Phys. Rev. Lett.* **101**, 250602 (2008).

[66] T. Nishino and K. Okunishi, Corner transfer matrix renormalization group method, *Journal of the Physical Society of Japan* **65**, 891 (1996).

[67] See Supplemental Material (SM) for additional details on fermionic iPESS techniques, numerical data, and algorithm benchmarks.

[68] H.-C. Jiang, Z.-Y. Weng, and T. Xiang, Accurate determination of tensor network state of quantum lattice models in two dimensions, *Physical review letters* **101**, 090603 (2008).

[69] H. Li and F. D. M. Haldane, Entanglement spectrum as a generalization of entanglement entropy: Identification of topological order in non-abelian fractional quantum hall effect states, *Physical review letters* **101**, 010504 (2008).

[70] J. I. Cirac, D. Poilblanc, N. Schuch, and F. Verstraete, Entanglement spectrum and boundary theories with projected entangled-pair states, *Phys. Rev. B* **83**, 245134 (2011).

[71] D. Poilblanc, N. Schuch, D. Pérez-García, and J. I. Cirac, Topological and entanglement properties of resonating valence bond wave functions, *Phys. Rev. B* **86**, 014404 (2012).

[72] D. Poilblanc, N. Schuch, and I. Affleck, SU(2)₁ chiral edge modes of a critical spin liquid, *Phys. Rev. B* **93**, 174414 (2016).

[73] K. Gawedzki, Wess-Zumino-Witten conformal field theory, in *Constructive Quantum Field Theory II*, edited by G. Velo and A. S. Wightman (Springer US, Boston, MA, 1990) pp. 89–120.

[74] S.-S. Gong, W. Zhu, J.-X. Zhu, D. N. Sheng, and K. Yang, Global phase diagram and quantum spin liquids in a spin-1/2 triangular antiferromagnet, *Physical Review B* **96**, 075116 (2017).

[75] A. Wietek and A. M. Läuchli, Chiral spin liquid and quantum criticality in extended $s=1/2$ heisenberg models on the triangular lattice, *Physical Review B* **95**, 035141 (2017).

[76] M. Rader and A. M. Läuchli, Finite correlation length scaling in lorentz-invariant gapless iPEPS wave functions, *Phys. Rev. X* **8**, 031030 (2018).

[77] P. Corboz, P. Czarnik, G. Kapteijns, and L. Tagliacozzo, Finite correlation length scaling with infinite projected entangled-pair states, *Phys. Rev. X* **8**, 031031 (2018).

[78] J. Hasik, D. Poilblanc, and F. Becca, Investigation of the n  el phase of the frustrated heisenberg antiferromagnet by differentiable symmetric tensor networks, *SciPost Physics* **10**, 012 (2021).

[79] F. Ferrari, S. Niu, J. Hasik, Y. Iqbal, D. Poilblanc, and F. Becca, Static and dynamical signatures of dzyaloshinskii-moriya interactions in the heisenberg model on the kagome lattice, *SciPost Physics* **14**, 139 (2023).

[80] J. Hasik and P. Corboz, Incommensurate order with translationally invariant projected entangled-pair states: Spiral states and quantum spin liquid on the anisotropic triangular lattice, *Physical Review Letters* **133**, 176502 (2024).

[81] H.-J. Liao, Z.-Y. Xie, J. Chen, Z.-Y. Liu, H.-D. Xie, R.-Z. Huang, B. Normand, and T. Xiang, Gapless spin-liquid ground state in the $s=1/2$ kagome antiferromagnet, *Physical review letters* **118**, 137202 (2017).

[82] A. Szasz, J. Motruk, M. P. Zaletel, and J. E. Moore, Chiral spin liquid phase of the triangular lattice hubbard model: a density matrix renormalization group study, *Physical Review X* **10**, 021042 (2020).

[83] B.-B. Chen, Z. Chen, S.-S. Gong, D. Sheng, W. Li, and A. Weichselbaum, Quantum spin liquid with emergent chiral order in the triangular-lattice hubbard model, *Physical Review B* **106**, 094420 (2022).

[84] L. F. Tocchio, A. Montorsi, and F. Becca, Hubbard model on triangular n-leg cylinders: Chiral and nonchiral spin liquids, *Physical Review Research* **3**, 043082 (2021).

[85] L. Devos and J. Haegeman, *Tensorkit. jl*: A julia package for large-scale tensor computations, with a hint of category theory, *arXiv preprint arXiv:2508.10076* (2025).

[86] M. Rams, G. W  jtowicz, A. Sinha, and J. Hasik, *Yastn*: Yet another symmetric tensor networks; a python library for abelian symmetric tensor network calculations, *SciPost Physics Codebases* , 052 (2025).